

Diffusion and escape from polygonal channels: extreme values and geometric effects

Jordan Orchard¹, Lamberto Rondoni^{2,3}, Carlos
Mejía-Monasterio⁴, Federico Frascoli¹

¹ Department of Mathematics, School of Science, Swinburne University of
Technology, H38, PO Box 218, Hawthorn, Victoria 3122, Australia

² Department of Mathematical Sciences, Politecnico di Torino, Corso Duca degli
Abruzzi 24, I-10129 Torino, Italy

³ Istituto Nazionale di Fisica Nucleare, Sezione di Torino, Turin, Italy,

⁴ School of Agricultural, Food and Biosystems Engineering, Technical University of
Madrid, Av. Complutense s/n, 28040 Madrid, Spain

E-mail: jorchard@swin.edu.au, lamberto.rondoni@polito.it,
carlos.mejia@upm.es, ffrascoli@swin.edu.au

January 2021

Abstract. Polygonal billiards are an example of pseudo-chaotic dynamics, a combination of integrable evolution and sudden jumps due to conical singular points that arise from the corners of the polygons. Such pseudo-chaotic behaviour, often characterised by an algebraic separation of nearby trajectories, is believed to be linked to the wild dependence that particle transport has on the fine details of the billiard table. Here we address this relation through a detailed numerical study of the statistics of displacement in a family of polygonal channel billiards with parallel walls. We show that transport is characterised by strong anomalous diffusion, with a mean square displacement that scales in time faster than linear, and with a probability density of the displacement exhibiting exponential tails and ballistic fronts. In channels of finite length the distribution of first-passage times is characterised by fat tails, with a mean first-passage time that diverges when the aperture angle is rational. These findings have non trivial consequences for a variety of experiments.

Keywords: Polygonal billiards, Anomalous diffusion, Strong anomalous diffusion, First-passage times, Survival probability.

Submitted to: *JSTAT*

1. Introduction

The transport properties of assemblies of highly confined particles in nanochannels greatly differ from those of macroscopic fluid systems. In confined geometries, the interactions between the particles and the channel walls occur with frequency and magnitude that are comparable (when not greater) than those associated with particle-particle interactions, hindering the realisation of Local Thermodynamic Equilibrium (LTE) on which the standard thermodynamic laws like Fick's law of diffusion are based [1, 2]. When confinement is particularly pronounced, the conditions for the validity of kinetic theory fail as well. For instance, macroscopic containers may keep a gas in different equilibrium states even if they are connected by channels that allow the flow of particles but prevent the interactions among them due to geometry, like in Knudsen gases [3, 4]. Geometry effects due to confinement may also prevent the decay of microscopic correlations that is required for locality to hold, allowing hydrodynamic interactions that commonly lead to an enhancement in the fluid flow [5, 6, 7, 8, 9].

When the dimensions of the container are comparable to the molecular characteristic scales, transport drastically slows down, with single-file diffusion being a prototypical example [10, 11, 12]. There are other cases where instead densely packed systems yield a strong enhancement of the rate of diffusion [13, 14], and where anomalies arise as the result of collective mediated interactions due to confinement, external driving and macromolecular crowding [15, 16]. Colloidal systems out of equilibrium and small biological systems [17, 18] share similar features.

A prototypical example of transport in confined geometries is that of diffusion through narrow channels. Understanding whether transport through nano channels is diffusive or anomalous has gained increasing interest as it would allow the control of a wide variety of phenomena and applications, such as ion transport across the cell membrane [19], drug delivery [20], nanopore sensing [21], ion transport control for energy harvesting [22], water flow in carbon nanotubes [23], diffusion of waves in corrugated channels [24], single photons in optic fibers [25] among many others.

Denoting by $x(t)$ the position of a tagged particle at time t , transport of matter is customarily defined in terms of the fluctuations of the displacement $\Delta x = x(t) - x(0)$ of the particles constituting the fluid. Macroscopic transport within stationary media is commonly diffusive, and the displacement is described by the diffusion equation, whose solution for a localised initial density is a time dependent Gaussian distribution

$$P(\Delta x, t) = 1/\sqrt{2\pi dDt} \exp(-\Delta x^2/2dDt), \quad (1)$$

where d is the spatial dimension, and D is the diffusion coefficient. The size of the fluctuations of the particles' displacement is then given by the variance of the displacement, *i.e.* the Mean Square Displacement (MSD). In the case of Eq. (1), the MSD is given by:

$$\langle (x(t) - x(0))^2 \rangle = 2dDt. \quad (2)$$

If the MSD is not described by Eq. (2), then transport is called anomalous. One of the

aims of the present study is to characterise the anomalous transport associated with a specific family of billiards and discuss the role of geometry in a number of important properties that describe the billiards' dynamics.

In this paper we revisit the problem of particle transport in polygonal billiard channels. Billiards constitute an attractive basis to study a broad range of fundamental problems in statistical mechanics, in particular transport in confined geometries [26, 27]. Mathematically, a billiard is a d -dimensional dynamical system, representing one point particle that moves freely inside a compact domain, the so-called table $\mathcal{B} \subset \mathbb{R}^d$, and that is specularly reflected at the boundary $\partial\mathcal{B}$ of \mathcal{B} . The boundary is required to be piecewise smooth, except in a countable number of points. Multiple extensions of this simple scenario have been considered, including interacting particles [26, 28], time-dependent boundaries [29], thermostated dynamics [30, 31], stochastic boundaries [32], and boundary with holes [33].

Normal diffusive transport as described by (2) is usually encountered in dispersing and semi-dispersing billiards [34, 35], whose dynamics is characterised by positive Lyapunov exponents. In contrast, polygonal billiards have zero Lyapunov exponents. The separation of nearby trajectories, which is always slower than exponential, is due to the corners of the polygon associated to the existence of singular conical points in the billiard flow. The question on whether diffusive transport can be obtained in polygonal channels was thoroughly analysed in several works [7, 8, 9, 36, 37]. Transport was found to range from diffusive to ballistic, with abrupt and unpredictable variations of its details under variations of the geometric parameters.

We focus on those fine details for a particular family of polygonal billiard channels with parallel boundaries defined in Section 2. The statistics of the particle displacement is analysed in Section 3. Later in Section 4, we analyse the transmission of particles through channels of finite length and discuss the statistics of survival probabilities and first-passage times to the channel's exits. Finally in Section 5 we report our conclusions. Our main results are on the interplay between ballistic fronts and the wild dependence that transport properties have on the geometric parameters. Additionally, we show that the distribution of first passage times for channels of finite width is broad, with a mean first passage time that diverges for simple rational billiards.

2. Polygonal billiard channels

We consider periodic polygonal billiard channels, made of identical copies of a fundamental cell with parallel walls, vertically shifted of a distance d with respect to each other, as shown in Fig. 1. The fact that the walls are parallel is an important feature of our systems and will have interesting consequences, as will be seen shortly.

For all geometries, the horizontal width of the cell is set to $2\delta x = 1$. Therefore, two parameters suffice to specify the shape of the channel: the vertical shift $d > 0$ and the aperture angle $\alpha \in (0, \pi)$. When the channel width $d > \delta x \cot(\alpha/2)$ the horizon is infinite, meaning that a particle trajectory can move for arbitrarily long distances

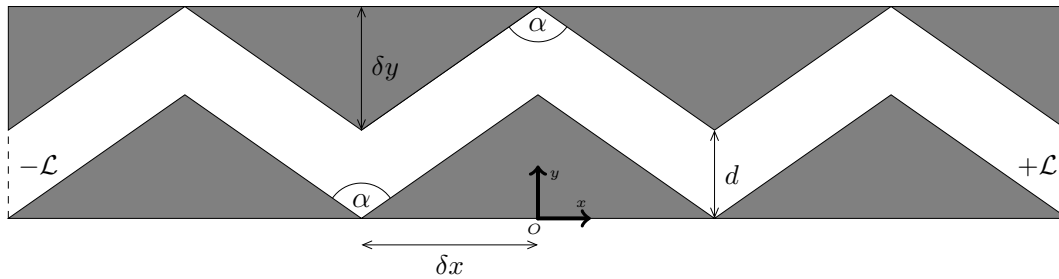


Figure 1. Polygonal channel made of (three) identical copies. The geometry of the fundamental cell is determined by the aperture angle α and the cell width d , with a cell length fixed to $2\delta x = 1$. The boundary height is given by $\delta y = \delta x \cot \alpha/2$. Setting the central cell at the origin, a channel made of L cells extends to $x = \pm\mathcal{L}$, with $\mathcal{L} = \lfloor \frac{L}{2} \rfloor + \frac{1}{2}$, and $\lfloor \cdot \rfloor$ being the floor function.

without hitting the channel boundaries. Inside the channel, point particles move with constant speed along straight lines until they elastically collide with the boundary, where their trajectories are specularly reflected.

As noted earlier, the dynamics of polygonal billiards have zero Lyapunov exponents. Whether this should imply faster or slower transport is not obvious. In the case of dispersive billiards, which have positive Lyapunov exponents, a well-understood example is the Lorentz gas, which was intensively investigated a few decades ago. In that system, transport can be understood in terms of unstable periodic orbits [38, 39], which subdivide in confined and ballistic orbits, the latter being periodic only modulo the periodic lattice spacing. Confined orbits do not contribute to transport, whereas ballistic ones do: their combined contribution results in normal diffusion if the horizon is finite. The strict hyperbolicity of the system causes generic trajectories to always come close to some periodic one, but only for a short time in the vicinity of a given periodic orbit, thus efficiently mixing velocities.

Contrary to the Lorentz gas, intuition on polygonal channels' dynamics is not straightforward, one reason being that parallel walls cause families of bouncing ball modes to be present. These are periodic trajectories that collide with the same pair of parallel wall segments, giving a vanishing contribution to transport. Differently from the chaotic case, escape from a narrow neighbourhood of a bouncing ball orbit is very slow and jeopardises the mixing of velocities. Only near the polygon's corners trajectories are separated, and velocities substantially change. This implies that trajectories initially in the neighbourhood of a bouncing ball orbit, move slowly away from that orbit, hence, at least initially, they give a small contribution to the transport properties. This behaviour is more prominent in rational polygons, where the number of possible velocity orientations is finite, *e.g.* just four for $\alpha = \pi/2$. A similar phenomenon, however, occurs for the ballistic orbits, *i.e.* those that are periodic only up to periodic lattice vector translation. These trajectories are very fast, and do not quickly decorrelate from orbits that start in their vicinity, which overall results in a large contribution to transport. Which of the two effects dominates transport and how it is related to the geometry of

the system is a hard open question, which we partly unravel in this paper.

What one observes is that the velocity vector explores a larger set of discrete orientations in irrational polygons than in rational ones. With parallel walls, the set of orientations of the particle velocity does not contract or expand upon successive collisions with the billiard boundary, as they instead do with non parallel walls. This leads to a propensity of sets of trajectories to persist along highly correlated unidirectional flights. While it is not clear whether the set of orientations is dense, the exploration of possible orientations is instead extremely slow [40, 7].

This polynomial separation of trajectories inspired a simple map, the Slicer Map [41], to understand the properties of transport. The slicer map exhibits strong anomalous diffusion [42] and, as recently shown, the map and polygonal billiard channels belong to a universality class of dynamics asymptotically dominated by a ballistic front [37]. It is important to note that trajectories travelling arbitrarily long distances before reversing do act effectively as ballistic fronts. Interestingly, such ballistic fronts do not require an infinite horizon but exist with finite horizon as in the case of periodic dispersive billiards. But, unlike that case, they are only weakly unstable because collisions with the boundary are not defocusing: the result is an overall poorly mixing dynamics that is much harder to characterise and globally more unpredictable than chaotic dynamics [7].

One of our main goals in this work is to study the statistics of particle displacement and its relation with the two free parameters d and α that determine the billiard's geometry. There are two main characteristics of the geometry that have a strong impact on transport: whether the angle α is a rational or irrational multiple of π and whether the horizon is finite or infinite. Hereafter, when referring to α as being rational or irrational, we will mean that α/π is rational or irrational. Unless otherwise specified, for each rational angle $\alpha_{\text{R}} = \frac{p}{q}\pi$, with $p, q \in \mathbb{Z}$ we will consider its irrational counterpart defined as $\alpha_{\text{I}} = (\varphi - \frac{3}{5})\alpha_{\text{R}}$ where $\varphi = (\sqrt{5} + 1)/2$, so that α_{R} and α_{I} differ by less than 2%.

Furthermore and unless otherwise specified, we consider only two different channel widths: $d = 2\delta y$ for the infinite horizon and $d = \delta y/2$ for the finite horizon case, where $\delta y = \delta x \cot \alpha/2$ is the geometric width of the polygonal boundary (see Fig. 1). When $\delta y = 1$ the y -coordinate of the lower corners located at the integer values $x = n$ coincide with that of the upper corners at $x = n + 1/2$ and the horizon is critical.

3. Particle displacement

In this Section we study the statistics of the displacement $\Delta x(t) = x(t) - x(0)$ for noninteracting particles moving in a parallel polygonal channel of infinite length. At the initial time, $t = 0$, the particles positions $(x(0), y(0))$ are uniformly distributed inside the central cell, and the velocity vectors all have unit magnitude, with their orientation forming an angle with the horizontal direction that is uniformly distributed over $[0, 2\pi)$.

3.1. Probability distribution

We focus first on the probability distribution function of the particle displacement $P(\Delta x, t)dt$, which is the probability that one particle is found at a distance Δx from its initial position and at a time between t and $t + dt$. We have numerically reconstructed $P(\Delta x, t)$, by computing the displacement $\Delta x(t)$ at different times t for an ensemble of particles. The shape of the probability density $P(\Delta x, t)$, and thus the properties of the particle transport in the channel, depend on the two free parameters d and α .

Transport is called scale invariant when the probability density scales in time as:

$$P(\Delta x, t) = \frac{1}{t^\gamma} P\left(\frac{\Delta x}{t^\gamma}\right) \quad (3)$$

with γ a positive fixed parameter. Here $t^{-\gamma}$ defines the proper scaling length of the process. For processes with constant speed, γ must take values in $[0, 1]$. Then, a generalised diffusion coefficient can be defined as:

$$\mathcal{D} := \lim_{t \rightarrow \infty} \frac{\text{Var}[\Delta x(t)]}{2dt^{2\gamma}}, \quad \text{Var}[\Delta x(t)] = \langle \Delta x^2(t) \rangle - \langle \Delta x(t) \rangle^2. \quad (4)$$

Normal diffusion corresponds to $\gamma = 1/2$, sub-diffusion to $0 < \gamma < 1/2$ and super-diffusion to $1/2 < \gamma < 1$. For $\gamma = 1$ the transport is called ballistic. As a consequence of scale invariance, the moments of the displacement obey the following relation:

$$\begin{aligned} \langle |\Delta x(t)|^p \rangle &= \int_{-\infty}^{\infty} |\Delta x|^p P(\Delta x, t) d(\Delta x) \\ &= \int_{-\infty}^{\infty} |\Delta x|^p P\left(\frac{\Delta x}{t^\gamma}\right) d\left(\frac{\Delta x}{t^\gamma}\right) \\ &= t^{p\gamma} \int_0^{\infty} |u|^p P(u) du, \end{aligned} \quad (5)$$

where $u = \Delta x/t^\gamma$. Assuming that the distribution $P(u)$ is not broad, so that all its moments exist, the integral in the last line of Eq. (5) is finite and we obtain

$$\langle |\Delta x(t)|^p \rangle \sim t^{p\gamma}. \quad (6)$$

In particular, the mean-square displacement scales in time as $\langle (\Delta x(t))^2 \rangle \sim t^{2\gamma}$.

In order to analyse the scaling of the probability distribution function of the particles' displacement, we have numerically followed an ensemble of 10^6 trajectories, for a time $t = 10^5$, for four different polygonal channels: a rational polygon with $\alpha_R = \pi/2$ with finite ($d = \delta y/2$) and infinite ($d = 2\delta y$) horizons, as well as an irrational polygon with $\alpha_I = \frac{\pi}{2}(\varphi - \frac{3}{5})$, for the same wall separation d . In Fig. 2 we show the probability distribution of the particle displacement computed at six different times: $t = \{1000, 10000, 25000, 50000, 75000, 100000\}$. Within the fairly large space and time scales that we have explored, we found that $P(\Delta x, t)$ is indeed not broad, and has exponential or multi exponential tails, that largely dominate the distribution. Moreover, $P(\Delta x, t)$ is also scale-invariant and, interestingly, the scaling parameter γ substantially depends only on the aperture angle α , whereas its dependence on d appears to be negligible. We find that the scaled distributions do asymptotically collapse into the same

master function with $\gamma = \gamma_R \approx 5/6$ and $\gamma = \gamma_I \approx 0.91$ for the rational and irrational polygons defined above. In the following section, we will consider the dependence on the aperture angle in more detail.

At finite times and large displacements, we observe that the distribution contains structures that are characteristic of ballistic fronts, with peaks of higher probability that move away from the center as time elapses. Interestingly, these ballistic fronts are present for all four cases, regardless of the horizon being finite or infinite. The position of the ballistic fronts is indicated by arrows in the upper left panel of Fig. 2.

The existence of ballistic fronts means that the scaling of Eq. (3) has to be complemented by a second contribution $\mathcal{F}(\Delta x, t)$ such that

$$\mathcal{F}(\Delta x, t) = \frac{1}{t} \mathcal{F}\left(\frac{\Delta x}{t}\right) \quad (7)$$

satisfies a ballistic scaling (see *e.g.* Ref. [43]). Clearly, $\mathcal{F}(\Delta x, t)$ is a sub leading contribution describing the behaviour at large displacements, *i.e.* $t^\gamma \ll \Delta x < t$, with appropriate scaling velocities. The collapse described by the leading scale-invariant contribution of Eq. (3) is then observed for displacements $\Delta x/t^\gamma$ smaller than the scaled position of the ballistic front, as expected.

Furthermore, we also observe that the bulk of the distributions are different: while for the rational polygons the centers of the distributions are spikelike, for the irrational polygons they are rounded. We notice that the bulk of the distribution, which in scaled units is defined by $\Delta x/t^\gamma < 1$, has the same dependence as its tails. These quantitative and qualitative differences between rational and irrational polygons have been found for all geometries considered here.

Looking at the evolution of the distributions one intuitively realises that in polygons with infinite horizon the distribution spreads more rapidly than those with finite horizon, because the progression in time is essentially determined by the speed of the ballistic front.

In Fig. 3 we plot the probability density of the particle displacement using a ballistic scaling, obtained with an exponent $\gamma = 1$. The scaling variable $\Delta x/t$ corresponds in this case to the speed of the front that we denote as v_{bal} : this is useful to distinguish the features of the distribution that scale ballistically.

Let us discuss first the rational polygon (left column of Fig. 3). In scaled units $\Delta x/t$ the position of the different peaks indicated by the arrows in Fig. 2 do collapse (as indicated in Fig. 3 by the vertical dashed lines), thus confirming that they correspond to a ballistic front. For the rational polygon with infinite horizon, the speed of the ballistic front is approximately $v_{\text{bal}} \approx 2/3$. With finite horizon, the existence of a ballistic front is also confirmed, with a different speed $v_{\text{bal}} \approx 1/2$. Moreover, the fastest widening trajectories with finite horizon correspond precisely to the ballistic front, while in the case of infinite horizon there exist trajectories that spread faster: those that undergo no collisions and have speed $\Delta x/t = 1$ (indicated by the arrow in the upper left panel of Fig. 3). Without acceleration, no trajectory can be faster than this free-flight front, which arise as soon as the channel's horizon is infinite and independently of the angle α .

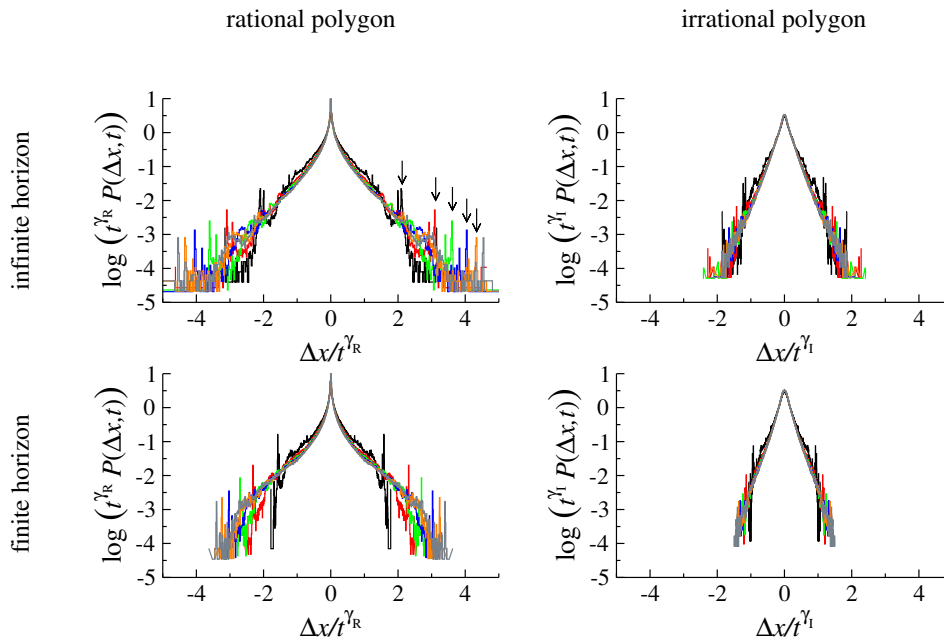


Figure 2. Probability density of the particle displacement $P(\Delta x, t)$ multiplied by t^γ , plotted as a function of scaled variable $\Delta x/t^\gamma$ obtained from 10^6 particle trajectories. Each histogram corresponds to $t = 1000$ (black), 10000 (red), 25000 (green), 50000 (blue), 75000 (orange), and 100000 (grey). The probability density is shown for four different billiards as indicated by the labels: rational polygon $\alpha_R = \pi/2$ and the corresponding irrational polygon α_I , finite horizon with $d = \delta y/2$ and infinite horizon for $d = 2\delta y$. The scaling used was $\gamma_R = 5/6$ for the rational polygon and $\gamma_I = 0.91$ for the irrational polygon. The arrows in the upper left panel indicate the position of the ballistic front at different times (see Fig. 3).

In addition, the fraction of such fastest trajectories decreases with t , since it approaches the set of exactly horizontal trajectories.

Turning our attention to the irrational polygon, we do indeed see the free-flight ballistic front when the horizon is infinite, in addition to the slower ballistic front. The latter varies with the geometry of the billiard, but it exists whether the horizon is finite or infinite. We speculate that this ballistic front is due to the trajectories that initially are in a close neighbourhood of the shortest periodic orbit of the billiard. As such, other fronts are expected to exist and indeed we observe certain features of the probability distribution that collapse in position under the ballistic scaling. This may also explain the different velocity of the front for different geometries of the billiard. Given the differences between rational and irrational polygons, it comes as a surprise that the front speed seems to depend strongly on the channel's width, but apparently only mildly on whether the polygon is rational or not.

To study this further, we have numerically evaluated the speed of the ballistic front for the rational $\alpha = \pi/2$ polygonal channel and its irrational counterpart, for different widths. The results are shown in Fig. 4, where the dark blue squares refer to the rational polygon, and the light yellow circles to the irrational one. Opening the horizon leads to

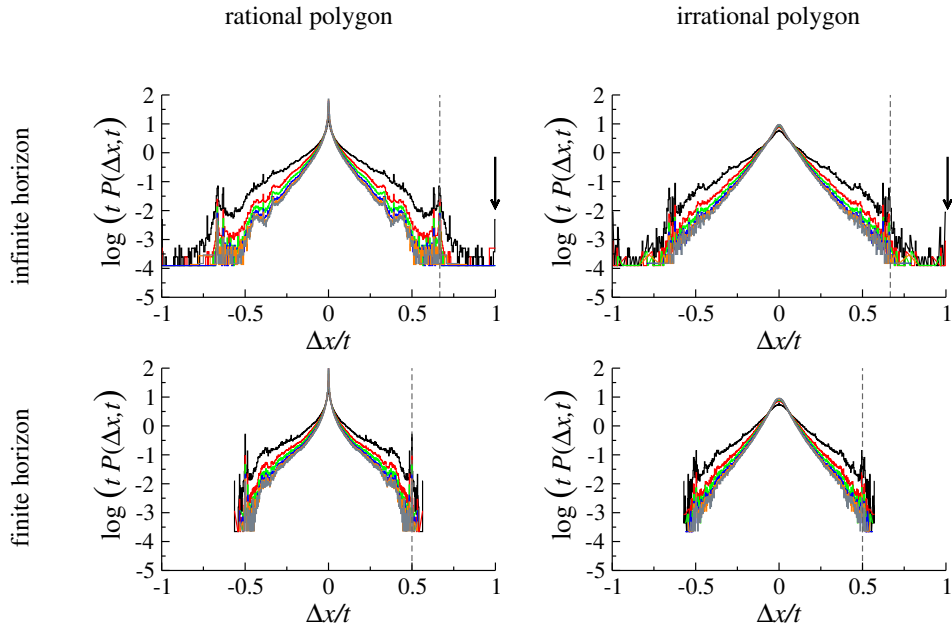


Figure 3. Ballistic scaling of the probability density of the particle displacement $P(\Delta x, t)$ shown in Fig. 2. The dashed vertical lines are a guide to the eye, indicating the value of the speed of the ballistic front $v_{bal} = \Delta x/t$. The arrow in the upper left panel indicates the non-collisional ballistic front with unit speed.

a sharp transition in the behaviour of the speed of the ballistic front: for finite horizon $d < \delta y$, the speed of the ballistic front does saturate to approximately $1/2$. When the horizon opens, the speed v_{bal} grows monotonically toward its upper bound $v_{bal} = 1$. From a fit to power-law, we obtain that the speed approaches unity as

$$v_{bal} = 1 - 0.52 \left(\frac{d}{\delta y} \right)^{-2/3}, \quad \text{for } \frac{d}{\delta y} > 1, \quad (8)$$

as shown by the solid curve in Fig. 4. As a final remark we note that the ballistic front of the polygonal channel is mildly affected by whether the angle is rational or irrational. However, recalling that $(\varphi - 3/5) \approx 1$, and that the angles compared in Fig. 4 are very similar in value, we cannot discard the possibility that v_{bal} could depend on the value of the aperture angle in a stronger fashion. Moreover, conjecturing that the speed of the ballistic front depends on the length of the simplest periodic orbit, v_{bal} should depend evenly on all the parameters of the geometry of the billiard.

3.2. Mean-square displacement

In the previous section we have analysed the properties of the probability distribution of the particle displacement and established that transport is anomalous, with $P(\Delta x, t)$ having exponential tails and a super-diffusive scaling, with an exponent that depends on whether the angle is rational or not. In this section we further explore the dependence of transport on the aperture angle α , focussing on the mean-square displacement. For a scale-invariant probability distribution, the mean-square displacement scales

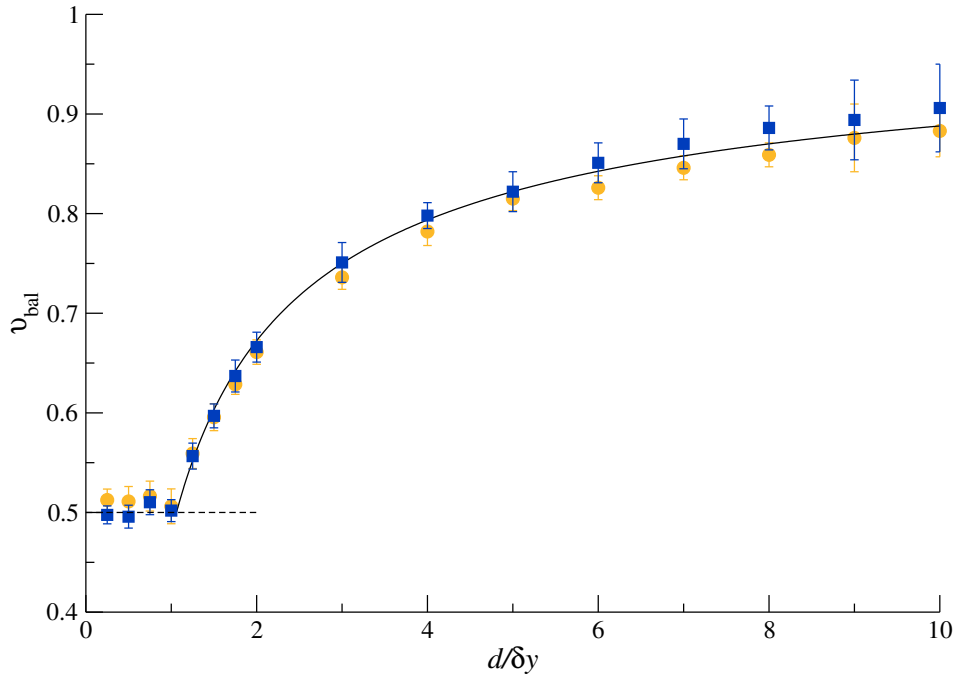


Figure 4. Velocity of the ballistic front as a function of the width of the channel d in units of δy for the irrational angle $\alpha = \frac{\pi}{2} (\phi - \frac{3}{5})$ (light yellow circles) and the rational angle $\alpha = \frac{\pi}{2}$ (dark blue squares). The dashed line indicates the value $v_{\text{bal}} = 1/2$. The solid curve corresponds to the function $v_{\text{bal}} = 1 - 0.52(d/\delta y)^{-2/3}$.

asymptotically as a power-law of time $\langle(\Delta x(t))^2\rangle \sim t^\eta$, where the exponent η is related to the scaling exponent of the probability distribution as $\eta = 2\gamma$ (see Eq. (11)).

We have numerically computed the mean-square particle displacement for polygonal channels with a finite horizon, $d = \delta y/2$, and different rational and irrational values of the angle α . The scaling exponent η is obtained from a fit to power-law of $\langle x^2(t) \rangle$ in the large time limit. The angles were chosen as rational values between $\pi/12$ and $11\pi/12$.

We show in Fig. 5 the power exponent η of the mean-square particle displacement for different angles α , in blue crosses rational polygons and in red circles their irrational counterparts. For $\alpha = \pi/2$ and $\alpha = \frac{\pi}{2} (\varphi - \frac{3}{5})$ we obtain $\eta = 1.662 \pm 0.006$ and $\eta = 1.825 \pm 0.006$ respectively, in agreement with the values of γ_R and γ_I obtained in the previous section.

Moreover, for all the parameters considered, the transport in parallel walls polygonal channels is found to be super-diffusive. Restricted to rational polygons, η seems to monotonically increase for $\alpha \geq \pi/3$. At smaller angles the power scaling η concentrates at values around 1.78. We recall that for $\alpha = \pi$ the corners of the polygonal channel disappear and the channel becomes rectilinear, yielding $\eta = 2$. Therefore, we expect that $\lim_{\alpha \rightarrow \pi} \eta = 2$ irrespective if the angle is rational or not, as confirmed by Fig. 5. In the irrational polygons, transport appears to be more stable than in the rational polygons, with a power scaling concentrated inside a small interval around $\eta \approx 1.84$.

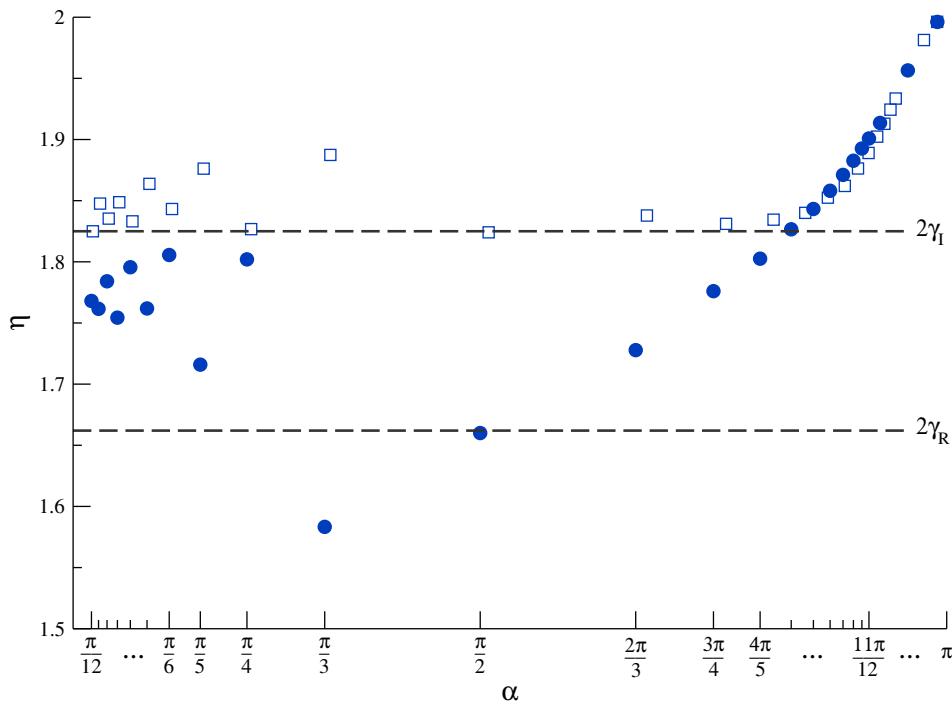


Figure 5. MSD scalings η for rational (solid circles) and irrational billiards (open squares). Simulations involved 10^6 trajectories of length $t = 10^6$ for irrational α 's and $t = 10^5$ for the rational α 's. A finite horizon channel with $d = \delta y/2$ was used for all cases, but a similar behaviour occurs for infinite horizons. The horizontal dashed lines indicate the expected values for the MSD for $\alpha = \pi/2$ from the corresponding scalings γ_R and γ_I of the probability distribution function. Statistical errors are of the same magnitude as the symbols' size.

As a final remark we notice that the numerical convergence of the MSD statistics of the irrational polygons for small aperture angles $\alpha \lesssim \pi/4$, is drastically slower than for larger angles. The properties of the convergence to the asymptotic transport and how they are affected by the geometry deserves further investigation.

3.3. Higher order moments

To complete the picture we have numerically computed higher order moments of the particle displacement $\langle |\Delta x(t)|^p \rangle$.

In Section 3.1 we found that the probability distribution of the particle displacement is scale invariant (see Eq. (3)), with a scaling x/t^γ that depends on the geometry of the billiard. The scale-invariance of $P(\Delta x, t)$ exhibiting exponential tails does hold for displacements that are shorter than the position of the ballistic front, namely in scaled units for

$$\frac{\Delta x}{t^\gamma} < v_{\text{bal}} t^{1-\gamma}. \quad (9)$$

Different scales determining the evolution of $P(\Delta x, t)$ commonly lead to strong anomalous diffusion characterised by a non-homogeneous scaling of the moments of

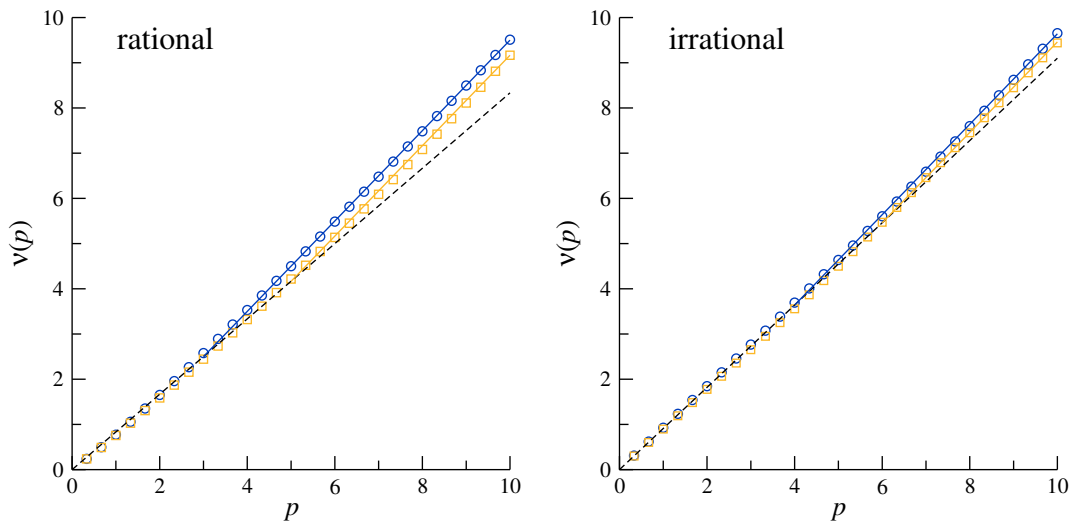


Figure 6. Spectrum of the moments of displacement of Eq. (11) for the same channels as in Fig. 2, rational polygon with $\alpha = \pi/2$, irrational polygon with $\alpha = \frac{\pi}{2}(\phi - \frac{3}{5})$, and finite horizon with $d = \frac{\delta y}{2}$ (dark blue circles), and infinite horizon for $d = 2\delta y$ (light yellow squares). In the left panel the lines are $5p/6$ (dashed), and $p-1/2$, $p-5/6$ (in solid). In the right panel the lines are $0.91p$ (dashed), and $p-0.36$, $p-0.54$ (in solid). Solid lines are shown with the same colour as the corresponding symbols.

the displacement with time. Strong anomalous diffusion, first described in Ref. [42], is characterised by the relation:

$$\langle |\Delta x(t)|^p \rangle \sim t^{\nu(p)}, \quad (10)$$

where the scaling exponent $\nu(p)$ is not linear in the moment's order p .

Strong anomalous diffusion was observed in Ref. [9] for general polygonal channels with finite and infinite horizon. There, the authors found that the moments of displacement can be subdivided in two branches: a scaling $\langle |\Delta x(t)|^p \rangle \sim t^{\nu_{\text{low}}}$ for low order moments $p < p^*$, and $\langle |\Delta x(t)|^p \rangle \sim t^{\nu_{\text{high}}}$ for $p > p^*$. This piecewise behaviour is characteristic of systems with two different dynamic scales [42] and was recently shown [37] that polygonal channels with infinite horizon belong to a broader class of universality of transport that is asymptotically dominated by ballistic fronts.

Here we find that, independently of the geometry of the polygon, transport is strongly anomalous, with a piecewise linear spectrum characterised by superdiffusion for moments of order $p \leq p^*$ and ballistic branch for higher moments. This is shown in Fig. 6, where we plot the scaling exponent

$$\nu(p) = \lim_{t \rightarrow \infty} \frac{\log \langle |\Delta x(t)|^p \rangle}{\log t} \quad (11)$$

for the same polygonal channels investigated in section 3.1. Consistently with the previous results, low order moments of the displacement with $p < p^*$ and $p^* > 2$,

scale as

$$\nu(p) = \begin{cases} \frac{5}{6} p & \text{for the rational polygon} \\ 0.91 p & \text{for the irrational polygon} \end{cases} \quad (12)$$

for arbitrary horizons. Higher order moments scale ballistically, with a threshold order p^* that depends on the geometry, as shown in Table 1. We conjecture that this behaviour is qualitatively observed for arbitrary values of α and of d . Moreover, Fig. 5 shows that for $\alpha < \pi$ the MSD scales slower than ballistic, which means that the threshold moment order is $p^* > 2$ independently of the geometry.

polygon	horizon	α	d	p^*	$\nu(p)$
rational	finite	$\frac{\pi}{2}$	$\delta y/2$	3	$p - \frac{1}{2}$
rational	infinite	$\frac{\pi}{2}$	$2\delta y$	5	$p - \frac{5}{6}$
irrational	finite	$(\varphi - \frac{3}{5}) \frac{\pi}{2}$	$\delta y/2$	4	$p - 0.36$
irrational	infinite	$(\varphi - \frac{3}{5}) \frac{\pi}{2}$	$2\delta y$	6	$p - 0.54$

Table 1. Asymptotic ballistic spectrum of the moments of the displacement $\nu(p)$ for $p > p^*$, for the four combinations investigated.

4. Transmission through polygonal channels of finite length

In the previous section we have shown that the transport across parallel walls polygonal channels is super-diffusive and dominated asymptotically by a (possibly more than one) ballistic front, at different speeds. In this section we investigate how transport is determined in channels of finite length for which the asymptotic regime is not available.

We have explored channels of finite length with ends located at positions $x = \pm\mathcal{L} = (\lfloor \frac{L}{2} \rfloor + \delta x)$, and act as absorbing boundaries. We recall that $L \geq 1$ is the number of polygonal cells composing the channel, $\lfloor \cdot \rfloor$ refers to the greatest integer that is less than or equal to the argument, and $\delta x = 1/2$. When a particle reaches one of the two ends, it escapes the channel and is removed from the dynamics.

As particles have constant speed, finite size effects will appear effectively at times larger than τ^* , the shortest time at which particles escape from the channel. If the horizon is infinite then $\tau^* = \lfloor \frac{L}{2} \rfloor$ exactly. At finite horizon, the shortest absorption time is determined by the fastest ballistic front for the given geometry, and is approximately $\tau^* = \mathcal{L}/v_{\text{bal}}$.

For finite channels, the moments of the particle displacement can be defined at time t as a conditional average over the particles that are still inside the channel. For a total number M of particles we define

$$\langle |\Delta x(t)|^p \rangle = \frac{1}{\mathcal{N}_t} \sum_{j=1}^M \chi_j(t) |\Delta x_j(t)|^p, \quad (13)$$

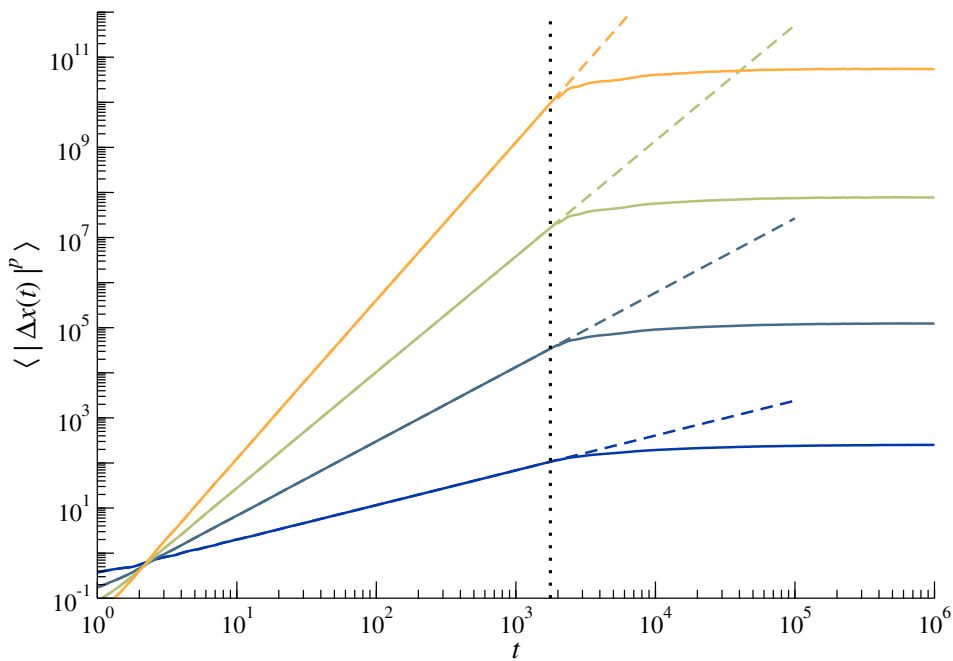


Figure 7. First four moments of the particle displacement $p = 1, \dots, 4$ (from dark blue to light yellow), for a channel composed of $L = 2001$ cells, $\alpha = \pi/2$ and $d = \delta y/2$ as per Eq. (13) (solid curves). The dashed curves correspond to the moments for the channel with infinite length. The dotted vertical line indicates the value of the shortest first-passage time $t = \tau^*$.

where the indicator function $\chi_j(t) = 1$ if by time t the j -th particle has not yet been absorbed, and $\chi_j(t) = 0$ otherwise. Then

$$\mathcal{N}_t = \sum_{j=1}^M \chi_j(t) \quad (14)$$

is the total number of particles that by time t have not escaped from the channel.

We have numerically computed Eq. (13) for a channel composed of $L = 2001$ rational cells with $\alpha = \pi/2$ and finite horizon $d = \delta y/2$. The first four moments are shown in Fig. 7, indicating a growth similar to that of the infinite channel (shown in dotted lines) upon saturation at $t = \tau^*$.

The saturation arises from the definition of the conditional sum in Eq. (13), and gives quantitative bounds for the moments, in particular for the mean-square displacement. In a channel of semi length \mathcal{L} , each particle contributes at most $|\mathcal{L} - x(0)|^2$ to the MSD: since the remaining particles in the channel give a smaller contribution, the MSD saturation value is of order $O(\mathcal{L}^2)$.

4.1. Statistics of first-passage times

The time τ^* corresponds to the shortest time at which a particle escapes the channel. In this section we explore the properties of this escape process in terms of the statistics of the first-passage time.

The concept of first-passage underlies a number of diverse stochastic processes, when the relevant information is represented by the first time at which the value of a random variable reaches a preset value [44]. The escape time of a given trajectory $x(t)$ can be seen as a first-passage time defined by:

$$\tau = \inf\{t : |x(t)| = \mathcal{L}\} , \quad (15)$$

where the inf is defined over the set of randomly initialised trajectories.

Consider a large set of trajectories parametrised by their initial position $\{(x_j(0), y_j(0))\}$ and initial velocity vector $\{\vec{v}_j : |\vec{v}_j| = 1\}$, and denote by τ_j the time t at which the j -th particle exits from one of the two channel's ends. Then borrowing the concept from stochastic dynamics, the normalised distribution $\Psi(\tau)$ of the escape times $\{\tau_j\}$ can be called the First-Passage Time Distribution (FPTD). For a randomly chosen initial condition, $\Psi(\tau)d\tau$ is the odds that such a trajectory will escape at a time between τ and $\tau + d\tau$. The mean escape time is then the Mean First-Passage Time (MFPT) defined as

$$\langle \tau \rangle = \int_0^\infty \tau \Psi(\tau) d\tau . \quad (16)$$

An interesting question is whether or not the Mean First-Passage Time (MFPT) characterises the typical escape time. As we learned in the previous section, the spreading of the trajectories occurs in different fashions, of which only part are ballistic. Therefore, it is not a priori clear if the MFPT is enough to describe the escaping process.

We have numerically computed the distribution of the first-passage time in channels of finite length and the same geometry as those studied in Section 3.1. As for the infinite channel, a large set of trajectories are randomly set in the central polygon cell, and for each of them we measure the time τ at which each trajectory reaches the channel ends. The histogram of this set of times is then used to numerically approximate the FPTD. The results are shown in Fig. 8 as solid dark blue curves.

At short times, the distribution $\Psi(\tau)$ has a cutoff at $\tau = \tau^*$, namely $\tau^* = \lfloor \frac{L}{2} \rfloor$ corresponding to the shortest free-flight trajectory in channels with infinite horizon, while for channels with finite horizon $\tau^* = \mathcal{L}/v_{\text{bal}}$, where v_{bal} is the speed of the fastest ballistic front. At later times, we observe an oscillating behaviour due to the escape of other slower ballistic fronts. More importantly, we note that $\Psi(\tau)$ decays asymptotically as a power-law of τ , meaning that the FPTD is broad and thus only a finite number of its lowest moments exist.

It is physically reasonable to describe our numerical results for $\Psi(\tau)$ with the distribution

$$\Psi(\tau) = \frac{\tau_0^\mu e^{-\tau_0/\tau}}{\Gamma(\mu) \tau^{1+\mu}} \quad (17)$$

where $\Gamma(\cdot)$ is the gamma function, τ_0 sets the cutoff of the distribution at short absorption times, and $\mu \geq 0$ is the so-called persistence exponent [45]. At short times, this distribution has an exponential cutoff that is a consequence of finite speed processes and, as our present results indicate, it is asymptotically dominated by a power-law tail.

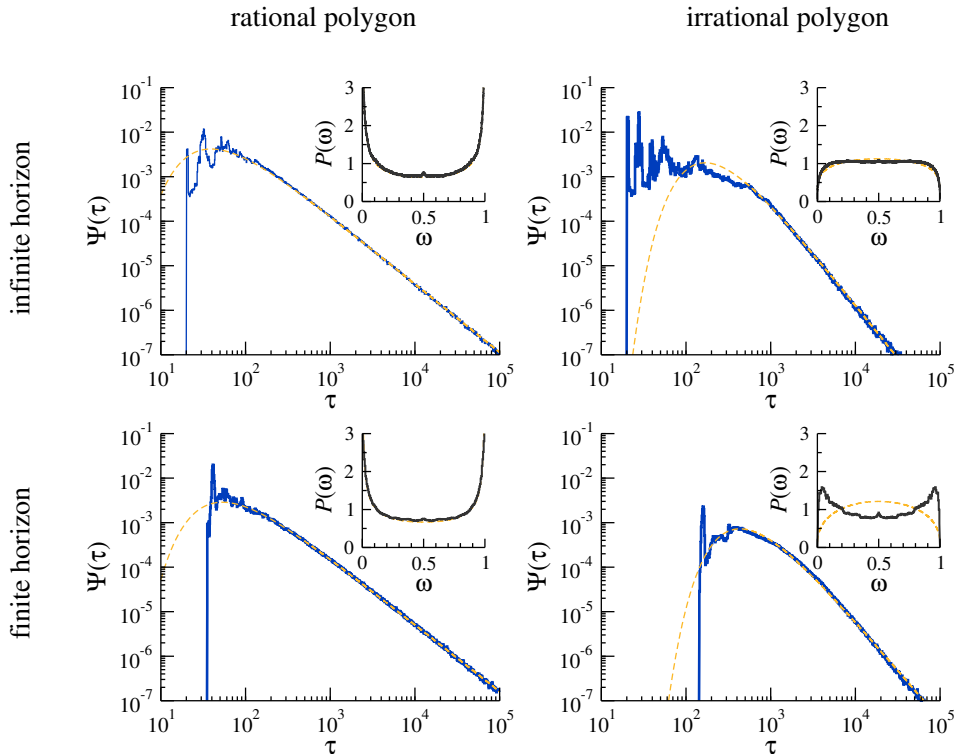


Figure 8. Distribution of the first-passage time $\Psi(\tau)$ (solid dark blue curves) to exit a finite channel of $L = 41$, for the same geometries as in Fig. 2: rational polygon with $\alpha = \frac{\pi}{2}$, irrational polygon with $\alpha = \frac{\pi}{2} (\phi - \frac{3}{5})$, finite horizon with $d = \frac{\delta y}{2}$ and infinite horizon for $d = 2\delta y$. Light yellow dashed curves are fits to Eq. (17) with fitting parameters as in Table 2. Insets: Numerically obtained distribution of the similarity index $P(\omega)$ for the corresponding geometries (solid black curves). The dashed light yellow curves correspond to Eq. (19).

Note that the distribution in Eq. (17) is exact for a one-dimensional Brownian motion in the semi-infinite line, with $\mu = 1/2$ and $\tau_0 = x_0^2/2D$, where x_0 is the starting position and D the diffusion coefficient [44]. The light yellow dashed curves in Fig. 8 correspond to the fit to Eq. (17), and the fitting parameters are reported in Table 2.

The sharper than exponential cutoff at short times, for the transmission across a polygonal channel, could be smoothed out by considering a higher power of the exponent τ_0/τ . Moreover, the short times oscillations are the result of the ballistic fronts and ultimately, to the underlying skeleton of the deterministic periodic orbits. Although Eq. (17) is not expected to be an exact description for our systems, the comparison is physically appealing, given its broad applicability. For instance, taking $\mu = 1 - 1/\alpha$, Eq. (17) provides a good approximation for the distribution of first-arrivals for Lévy flights, with Lévy index α , $1 < \alpha < 2$ [46]. Also, for $\mu = 1 - H$, Eq. (17) is a reasonable approximation for the FPTD of fractional Brownian motion with Hurst index H , where $0 < H < 1$ [47] (for a more detailed discussion about Eq. (17) see *e.g.* Ref. [48]).

Furthermore, the distribution in Eq. (17) is normalised, but for $0 \leq \mu < 1$ its first moment, the MFPT, does not exist. For $1 \leq \mu < 2$, the MFPT exists but the

polygon	horizon	α	d	τ_0	μ
rational	finite	$\frac{\pi}{2}$	$\delta y/2$	60	0.536
rational	infinite	$\frac{\pi}{2}$	$2\delta y$	80	0.498
irrational	finite	$(\varphi - \frac{3}{5})\frac{\pi}{2}$	$\delta y/2$	400	1.38
irrational	infinite	$(\varphi - \frac{3}{5})\frac{\pi}{2}$	$2\delta y$	960	1.2176

Table 2. Parameters τ_0 and μ obtained from the fit to Eq. (17), shown in Fig. 8 as dashed light yellow curves. Note the striking difference between rational and irrational channels.

variance of τ diverges, and so on. Observing the decay of the tails of $\Psi(\tau)$ in Table (2), we realise that for the rational polygonal channels, the MFPT, *i.e.* the mean time a particle takes to escape from the channel, diverges. This has important consequences for the transmission through a finite rational polygonal channel: even for a finite number of randomly initialised particles for which the MFPT to escape typically exists, a large variability in the absorption times is to be expected, yielding a meaningless MFPT [49]. This calls for a characterisation of the transmissibility that is not based on the mean escape time. In contrast, for irrational polygonal channels, the tail of $\Psi(\tau)$ decays faster than τ^{-2} , namely with $1 < \mu < 2$ so that the MFPT exists but the variance of the escape time diverges.

To study the variability in the escape times, we consider the similarity index ω studied in the context of first-passage times in Ref. [48]. Consider a set of N trajectories, and let $\{\tau_j\}$ denote the set of escape times corresponding to these trajectories. Then the similarity index is defined by the ratio between any of the escape times, say τ_j with $j \in \{1, \dots, N\}$, and mean escape time averaged over the set of N trajectories:

$$\omega_N = \frac{1}{N} \frac{\tau_j}{\langle \tau \rangle_N}, \quad (18)$$

where $\langle \tau \rangle_N = \frac{1}{N} \sum_{j=1}^N \tau_j$. This quantity probes the escape time of any given trajectory relative to the ensemble average over N trajectories. The domain of the similarity index is $\omega_N \in [0, 1]$ and is a random variable if the escape times $\{\tau_j\}$ are random variables. A low variability means that $\tau_j \approx \langle \tau \rangle_N$ for all the N trajectories, yielding $\omega_N \approx \frac{1}{N}$.

Here we explore the simplest expression for ω , namely for $N = 2$. Consider two trajectories with randomly chosen initial conditions. The first trajectory exits the channel at a time τ_1 while the second trajectory does it at a time τ_2 . Then, we have $\omega_2 = \tau_1/(\tau_1 + \tau_2)$ ‡. When all trajectories are absorbed at approximately the same time, $\omega_2 \approx 1/2$. When variations are large, *i.e.* $\tau_1 \gg \tau_2$ or $\tau_2 \gg \tau_1$, ω_2 attains a value close to 0 or to 1. For clarity in what follows we refer to ω_2 simply as ω .

The distribution of ω for the FPTD of Eq. (17) is given by [48]

$$P(\omega) = \frac{\Gamma(2\mu)}{\Gamma^2(\mu)} \omega^{\mu-1} (1-\omega)^{\mu-1}. \quad (19)$$

‡ Alternatively one can define $\omega_2 = \tau_2/(\tau_1 + \tau_2)$, which ultimately indicates that the probability distribution $P(\omega_2)$ is symmetric over its domain.

In the insets in Fig. 8 we show the corresponding numerically computed distributions $P(\omega)$ as solid black curves. For the rational polygonal channel, $P(\omega)$ has a characteristic “U” shape, with most probable values of ω at 0 and 1. Strikingly, the mean $\langle\omega\rangle = 1/2$ is the least probable value of the distribution. Such large variations of the absorption times are a consequence of the broadness of the FPTD.

For the irrational polygonal channels, the distribution of ω_2 is maximal at the mean $\langle\omega\rangle = 1/2$ for the infinite horizon, and is shaped like a “M” for the finite horizon. While the variability of the absorption times is markedly smaller than for the rational polygons, variations remain wild, as indicated by the almost flat profile of $P(\omega)$ near the center of the domain.

While the description in terms of $P(\omega)$ is only qualitative, it clearly reveals a remarkable difference between the rational polygon with $\alpha = \pi/2$ for which the MFPT diverges, and its irrational counterpart for which the MFPT exist but its variability is large to the extent that it does not characterise the escape time of a typical trajectory. In the next section we will generalise this observation to any rational and the irrational polygons.

As a final observation, we note that with the exception of the irrational polygon with finite horizon, Eq. (19), shown as the dashed light yellow curves in the insets of Fig. 8, is a reasonably good approximation of the numerically obtained $P(\omega)$. However, the “M” shape obtained for the irrational polygon with finite horizon cannot be described by Eq. (19), but is characteristic of a FPTD with power-law tails with an additional exponential cutoff at large τ [48], and its origin deserves further investigation.

4.2. Survival probability

In the previous Section we have seen that it is not possible to use the mean first-passage time to characterise the transmission through finite polygonal channels. In this Section we explore a global characterisation of the transmission process in terms of the survival probability. The survival probability $S(t)$ is the fraction of particles that have not yet escaped at time t , and is related to the FPTD through

$$\Psi(\tau) = -\frac{dS(\tau)}{d\tau} . \quad (20)$$

In our settings, the trajectories initially prepared in the central cell of the channel can indeed be physically seen as a short pulse of particles released in the center of the channel. By measuring the time at which the particles escape from the channel, we compute the survival probability $S(t)$ and characterise the transmission of the initial pulse, by defining a channel escape time τ_ϵ as the hitting time at which the survival probability decays to a value smaller than a given $\epsilon > 0$, namely

$$\tau_\epsilon = \inf \{t | S(t) < \epsilon\} . \quad (21)$$

We hence define the channel escape time as the time at which a fraction $(1 - \epsilon)$ of the total particles has escaped from the channel. Being an observable integrated over a

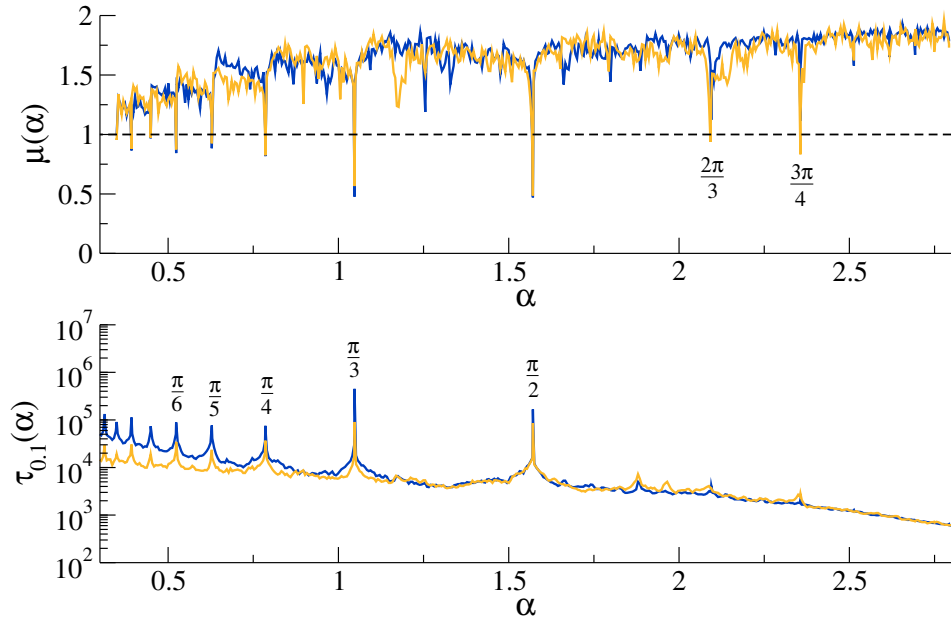


Figure 9. Top panel: Persistence exponent μ of the FPTD of Eq. (17) as a function of the aperture angle α , for a finite $d = \delta y/2$ (dark blue curve) and infinite $d = 2\delta y$ (light yellow curve) horizons. The horizontal dashed line indicates the value of μ above which the MFPT does not exist. Bottom panel: Corresponding escape time τ_ϵ of Eq. (21) for $\epsilon = 0.1$, as a function of the angle α . The results in this figure were derived from the survival probability obtained for each α , in a channel made of $L = 101$ cells.

finite time it is not affected by the divergence of the moments of $\Psi(\tau)$ and, interestingly, is one of the observables frequently measured in short pulse-response experiments [50].

Indeed, the inverse problem of inferring details of the geometry from the survival probability is a standard problem of scattering processes. In recent years it has been investigated in the so-called stochastic billiards, that are random processes derived from deterministic billiards [51, 52].

From Eqs. (17) and (20), the survival probability decays asymptotically as $S(\tau) \sim \tau^{\mu-2}$. This is in contrast to polygonal channels with non parallel walls, for which $S(\tau)$ was instead found to decay as a stretched exponential [36].

To explore the transmission in polygonal channels, we computed the statistics of the first-passage time as a function of the aperture angle α , for finite and infinite horizons. For all values of α , the survival probability (and thus the FPTD) decay asymptotically as a power-law of τ . From a fit to power-law, we obtained the exponent μ for the decay of the FPTD in Eq. (17), as a function of α , with the results shown in the top panel of Fig. 9.

Strikingly, for all simple rational polygons with aperture angle $\alpha = \pi/n$, and n an integer, the decaying exponent of the FPTD is $\mu < 1$, meaning that for all simple rational polygons the mean first-passage time diverges. The same is observed for $\alpha = 2\pi/3$ and $3\pi/4$. In contrast, other generic values, including the irrational polygons, have $1 < \mu < 2$ meaning that the MFPT exists, but the variance of the escape time diverges. This result

holds irrespectively of whether the channel's horizon is finite or infinite. We argue that the divergence of the MFPT is characteristic of rational polygons, and the reason why we do not observe this for all rational aperture angles α_R , lies in the infinite numerical accuracy needed to distinguish rational and irrational angles.

In the lower panel of Fig. 9, we show the channel escape time τ_ϵ for $\epsilon = 0.1$, namely the time at which the 90% of the initial particles have left the channel. The escape time is about an order of magnitude larger for simple rational polygons than for irrational ones, indicating that in rational polygonal channels transport drastically slows down, presumably because of the dense skeleton of periodic orbits characterising the channels' dynamics [53].

5. Conclusions

We have addressed the nature of mass diffusion in a family of open polygonal channels with parallel walls, analysing the statistics of particle displacement. While parallel channels have been subject to implicit or partial examination in previous works, the key questions of those studies concern the implications of normal transport in the absence of chaotic dynamics. This paper has instead a broader scope and has enabled insight into the fine tuning of transport properties with the details of the channel's geometry.

The probability distribution function of the particle displacement $P(\Delta x, t)$ is a combination of two contributions: a leading scale-invariant contribution with exponential tails describing the short fluctuations of the displacement, and a sub leading ballistic contribution, describing the evolution of the ballistic fronts. The scale of the leading contribution is $\Delta x/t^\gamma$, with a characteristic scale $\gamma < 1$ that depends on the geometry of the channel.

The ballistic front exists independently of the geometry of the channel. In particular, it is present irrespectively of whether the horizon is finite or infinite. The geometry determines the speed of the front. For an aperture angle $\alpha = \pi/2$ the speed seems to saturate when the horizon is finite, namely for $d < \delta y$, and converges to its upper bound $v_{\text{bal}} = 1$ as $d \rightarrow \infty$. We argue that this behaviour is qualitatively shown by arbitrary values of the aperture angle. Moreover, we speculate that the ballistic front is due to the trajectories that initially are in a close neighbourhood of the shortest periodic orbit of the polygonal billiard. That would explain not only the dependence of the speed of the ballistic front on the geometry of the channel but would also shed light on the strong variability observed on the transport properties. This question will be addressed in a forthcoming research.

In addition to the geometry dependent ballistic fronts, a free-flight ballistic front of unit speed appears, as soon as the horizon becomes infinite. However, the fraction of such fastest trajectories does necessarily decrease in time, since it approaches the set of exactly horizontal trajectories. With infinite horizon it would be possible in principle to describe the transport in polygonal channels in terms of the single big jump principle [43, 54]. However, our results suggest that the sub leading ballistic contribution vanishes

rapidly enough to affect the properties of transport.

For arbitrary geometry mass transport is super-diffusive, meaning that the MSD scales faster than linear in time. Polygons with rational aperture angle α show a MSD with a power scaling γ that increases smoothly with α , in contrast to irrational angles for which the power scaling is roughly constant. At large aperture angles both families converge to a ballistic behaviour as $\alpha \rightarrow \pi$. It still remains to be understood whether the coefficient for the MSD scaling of irrational parallel billiards, which appears to be almost constant throughout the range of the aperture angles we simulate, is an indication of a form of structural stability for these kinds of systems.

Exploring the spectrum of higher moments of the displacement we obtained that transport is characterised by strong anomalous diffusion, with moments higher than p^* scaling ballistically and lower moments exhibiting the same scaling as the MSD. For the geometries investigated, the threshold moment is $p^* > 2$ in all cases, meaning that the contribution of the ballistic fronts to the MSD vanishes sufficiently fast. In any case, the spectrum of moments of the displacement suggest that the transport in these polygonal channels belong to the universality class recently described in Ref.[37].

Borrowing concepts from stochastic dynamical systems, we have analysed the transmission of particles through finite channels under the light of first-passage time statistics. The distribution of FPT to leave the channel is dominated at short times by the ballistic fronts, and asymptotically decays as power-law, with a scaling that is determined by the channel's geometry. Fat tailed FPT distributions have important consequences on the variability of escape times. Strikingly, our numerical results suggest that when the aperture angle α is a simple rational, all moments of the distribution of FPT diverge, in particular the mean first passage time. For other angles the mean escape time exists, but its value does not represent the typical transmission due to the divergence of the escape time variance. The striking difference between statistics of the FPT for rational and irrational channels is interesting, pointing to highly dissimilar dynamics associated to heterogeneous structures of periodic and ballistic trajectories for the two cases. Notably, the consequences for experiments involving pulses and assemblies of particles are non trivial.

Findings discussed in the present work do not only pertain to highly idealised systems. Our investigation of transport properties, and in particular their dependence on the geometry of the channel, may help us elucidate the properties of realistic systems, for example those of transport and solution kinetics, or a variety of settings that involve diffusion and propagation of pulses, cells and tracers.

Acknowledgments

CMM does also acknowledges financial support from the Spanish Government grant PGC2018-099944-B-I00 (MCIU/AEI/FEDER, UE). LR acknowledges that the present research has been partially supported by MIUR grant Dipartimenti di Eccellenza 2018-2022 (E11G18000350001). JO and FF finally acknowledge financial support from the

Australian Research Grant DP180101512 and thank Swinburne University of Technology for the generous allocation of CPU time on the OzSTAR HPC cluster.

6. References

- [1] H J Kreuzer. *Nonequilibrium Thermodynamics and Its Statistical Foundations*. Clarendon Press, Oxford, 1983.
- [2] H Spohn. *Large scale dynamics of interacting particles*. Springer-Verlag, Berlin, 1991.
- [3] S R de Groot and P Mazur. *Non-equilibrium Thermodynamics*. Dover Publications Inc., New York, 1984.
- [4] Carlo Cercignani, Reinhard Illner, and Mario Pulvirenti. *The Mathematical Theory of Dilute Gases*. Springer, Berlin, 1994.
- [5] John A Thomas and Alan J H McGaughey. Water Flow in Carbon Nanotubes: Transition to Subcontinuum Transport. *Physical Review Letters*, 102(18):184502–4, May 2009.
- [6] Jiaye Su and Hongxia Guo. Effect of Nanochannel Dimension on the Transport of Water Molecules. *J. Phys. Chem. B*, 116(20):5925–5932, May 2012.
- [7] Owen G Jepps and Lamberto Rondoni. Thermodynamics and complexity of simple transport phenomena. *Journal of Physics A: Mathematical and General*, 39(6):1311–1338, January 2006.
- [8] Owen G Jepps, Carlo Bianca, and Lamberto Rondoni. Onset of diffusive behavior in confined transport systems. *Chaos: An Interdisciplinary Journal of Nonlinear Science*, 18(1):013127–14, March 2008.
- [9] David P Sanders and Hernán Larralde. Occurrence of normal and anomalous diffusion in polygonal billiard channels. *Physical Review E*, 73(2):23–9, February 2006.
- [10] D G Levitt. Dynamics of a single-file pore: Non-fickian behavior. *Physical Review A*, 8:3050, 1973.
- [11] K K Mon and J K Percus. Self-diffusion of fluids in narrow cylindrical pores. *The Journal of Chemical Physics*, 117(5):2289–2292, August 2002.
- [12] Alexander Berezhkovskii and Gerhard Hummer. Single-File Transport of Water Molecules through a Carbon Nanotube. *Physical Review Letters*, 89(6):155–4, July 2002.
- [13] Olivier Bénichou, Pierre Illien, Carlos Mejía-Monasterio, and Gleb Oshanin. A biased intruder in a dense quiescent medium: looking beyond the force–velocity relation. *Journal of Statistical Mechanics: Theory and Experiment*, 2013(05):P05008–30, May 2013.
- [14] P Illien, O Bénichou, C Mejia-Monasterio, G Oshanin, and R Voituriez. Active Transport in Dense Diffusive Single-File Systems. *Physical Review Letters*, 111(3):038102–5, July 2013.
- [15] Carlos Mejía-Monasterio and Gleb Oshanin. Bias- and bath-mediated pairing of particles driven through a quiescent medium. *Soft Matter*, 7(3):993, 2011.
- [16] Oleg Vasilyev, Olivier Bénichou, Carlos Mejía-Monasterio, Eric Weeks, and Gleb Oshanin. Cooperative behavior of biased probes in crowded interacting systems. *Soft Matter*, 13(41):7617–7624, October 2017.
- [17] Felix Höfling and Thomas Franosch. Anomalous transport in the crowded world of biological cells. *Reports on Progress in Physics*, 76(4):046602–51, March 2013.
- [18] R Metzler, J H Jeon, and A G Cherstvy. Non-Brownian diffusion in lipid membranes: Experiments and simulations. *BBA - Biomembranes*, pages 1–17, February 2016.
- [19] Giacomo Bruno, Nicola Di Trani, R Lyle Hood, Erika Zabre, Carly Sue Filgueira, Giancarlo Canavese, Priya Jain, Zachary Smith, Danilo Demarchi, Sharath Hosali, Alberto Pimpinelli, Mauro Ferrari, and Alessandro Grattoni. Unexpected behaviors in molecular transport through size-controlled nanochannels down to the ultra-nanoscale. *Nature Communications*, pages 1–10, April 2018.
- [20] Omaira M Sabek, Silvia Ferrati, Daniel W Fraga, Juliana Sih, Erika V Zabre, Daniel H Fine, Mauro Ferrari, A Osama Gaber, and Alessandro Grattoni. Characterization of a nanogland for the autotransplantation of human pancreatic islets. *Lab on a Chip*, 13(18):3675–14, 2013.

- [21] Lucile Reynaud, Aurélie Bouchet-Spinelli, Camille Raillon, and Arnaud Buhot. Sensing with Nanopores and Aptamers: A Way Forward. *Sensors*, 20(16):4495–29, August 2020.
- [22] Kai Xiao, Lei Jiang, and Markus Antonietti. Ion Transport in Nanofluidic Devices for Energy Harvesting. *Joule*, 3(10):2364–2380, October 2019.
- [23] Thomas Meersmann, John W Logan, Roberto Simonutti, Stefano Caldarelli, Angiolina Comotti, Piero Sozzani, Lana G Kaiser, and Alexander Pines. Exploring Single-File Diffusion in One-Dimensional Nanochannels by Laser-Polarized ^{129}Xe NMR Spectroscopy. *The Journal of Physical Chemistry A*, 104(50):11665–11670, December 2000.
- [24] Pierre Aschiéri, Valérie Doya, and Antonio Picozzi. Complex behaviour of a ray in a Gaussian index profile periodically segmented waveguide. *Journal of Optics A: Pure and Applied Optics*, 8(5):386–390, March 2006.
- [25] Ian S Osborne. Single photons for optic fibers. *Physiocal Review Letters*, 120, 2018.
- [26] Yakov G Sinai and N I Chernov. Ergodic properties of certain systems of two-dimensional discs and three-dimensional balls. *Russian Mathematical Surveys*, 42(3):181–207, October 2007.
- [27] Péter Bálint, Thomas Gilbert, Domokos Szász, and Imre Péter Tóth. What mathematical billiards teach us about statistical physics? *arXiv.org*, September 2020.
- [28] Steven Lansel, Mason A Porter, and Leonid A Bunimovich. One-particle and few-particle billiards. *Chaos: An Interdisciplinary Journal of Nonlinear Science*, 16(1):013129–13, March 2006.
- [29] Alexander Loskutov. Dynamical chaos: Systems of classical mechanics. *Physics-Uspokhi*, 50(9):939–964, September 2007.
- [30] Bill Moran, William G Hoover, and Stronzo Bestiale. Diffusion in a periodic Lorentz gas. *Journal of Statistical Physics*, 48(3):709–726, 1987.
- [31] J Lloyd, M Niemeyer, L Rondoni, and G P Morriss. The nonequilibrium lorentz gas. *Chaos*, 5:536–551, 1995.
- [32] Timothy Chumley, Renato Feres, and Hong-Kun Zhang. Diffusivity in multiple scattering systems. *Transactions of the American Mathematical Society*, 368(1):109–148, 2016.
- [33] Mark Demers, Paul Wright, and Lai-Sang Young. Escape Rates and Physically Relevant Measures for Billiards with Small Holes. *Communications in Mathematical Physics*, 294(2):353–388, November 2009.
- [34] L A Bunimovich. On the ergodic properties of nowhere dispersing billiards. *Communications in Mathematical Physics*, 65:295, 1979.
- [35] L A Bunimovich, Ya G Sinai, and N I Chernov. Statistical properties of two-dimensional hyperbolic billiards. *Russian Mathematical Surveys*, 46:47–106, 1991.
- [36] Daniel Alonso, A Ruiz, and I de Vega. Transport in polygonal billiards. *Physica D: Nonlinear Phenomena*, 187(1-4):184–199, January 2004.
- [37] Jürgen Vollmer, Lamberto Rondoni, Muhammad Tayyab, Claudio Giberti, and Carlos Mejía-Monasterio. Displacement autocorrelation functions for strong anomalous diffusion: A scaling form, universal behavior, and corrections to scaling. *Physical Review Research*, 3(1):013067, January 2021.
- [38] P Cvitanović, P Gaspard, and T Schreiber. Investigation of the lorentz gas in terms of periodic orbits. *Chaos*, 2:85–90, 1992.
- [39] G P Morriss and L Rondoni. Periodic orbit expansions for the lorentz gas. *Journal of Statistical Physics*, 75:553–584, 1994.
- [40] Eugene Gutkin. Billiards in polygons: Survey of recent results. *Journal of Statistical Physics*, 83(1):7–26, April 1996.
- [41] Lucia Salari, Lamberto Rondoni, Claudio Giberti, and Rainer Klages. A simple non-chaotic map generating subdiffusive, diffusive, and superdiffusive dynamics. *Chaos: An Interdisciplinary Journal of Nonlinear Science*, 25(7):073113–12, July 2015.
- [42] P Castiglione, A Mazzino, P Muratore-Ginanneschi, and A Vulpiani. On strong anomalous diffusion. *Physica D*, 134:75–93, August 1999.
- [43] Raffaella Burioni, Luca Caniparoli, and Alessandro Vezzani. Lévy walks and scaling in quenched

- disordered media. *Physical Review E*, 81(6):060101, June 2010.
- [44] Sidney Redner. *A Guide to First-Passage Processes*. Cambridge University Press, 1 edition, June 2007.
- [45] Alan J Bray, Satya N Majumdar, and Grégory Schehr. Persistence and first-passage properties in nonequilibrium systems. *Advances in Physics*, 62(3):225–361, June 2013.
- [46] Aleksei V Chechkin, Ralf Metzler, Vsevolod Y Gonchar, Joseph Klafter, and Leonid V Tanatarov. First passage and arrival time densities for Lévy flights and the failure of the method of images. *Journal of Physics A: Mathematical and General*, 36(41), October 2003.
- [47] Alex Hansen, Thor Engøy, and Knut Jørgen Måløy. Measuring Hurst exponents with the first return method. *Fractals*, 02(04):527–533, November 2011.
- [48] Carlos Mejía-Monasterio, Gleb Oshanin, and Grégory Schehr. First passages for a search by a swarm of independent random searchers. *Journal of Statistical Mechanics: Theory and Experiment*, 2011(06):P06022, June 2011.
- [49] Thiago G Mattos, Carlos Mejía-Monasterio, Ralf Metzler, and Gleb Oshanin. First passages in bounded domains: When is the mean first passage time meaningful? *Physical Review E*, 86(3):031143, September 2012.
- [50] Guy B Marin, Gregory S Yablonsky, and Denis Constales. *Kinetics of Chemical Reactions. Decoding Complexity*. Wiley-VCH, May 2019.
- [51] Renato Feres. Random walks derived from billiards. In Boris Hasselblatt, editor, *Dynamics, Ergodic Theory, and Geometry Dedicated to Anatole Katok*, pages 179–222. Cambridge University Press, Cambridge, January 2007.
- [52] Francis Comets, Serguei Popov, Gunter M Schütz, and Marina Vachkovskaia. Knudsen Gas in a Finite Random Tube: Transport Diffusion and First Passage Properties. *Journal of Statistical Physics*, 140(5):948–984, July 2010.
- [53] M Boshernitzan, G Galperin, T Kruger, and S Troubetzkoy. Periodic billiard orbits are dense in rational polygons. *Transactions of the American Mathematical Society*, 350(9):3523–3535, September 1998.
- [54] Alessandro Vezzani, Eli Barkai, and Raffaella Burioni. Rare events in generalized Lévy Walks and the Big Jump principle. *Scientific Reports*, 10(1):1–11, December 2020.